Bol. Soc. Paran. Mat.
©SPM – E-ISSN-2175-1188
SPM: www.spm.uem.br/bspm

(3s.) **v. 2026 (44) 4** : 1–23.
ISSN-0037-8712
doi:10.5269/bspm.80086

Casson Nanofluid Flow in Vertical Channel under Variable Viscosity and Thermal Conductivity with Viscous Dissipation Effects

Bhuvaneshwari R. Havaleppanavar, SYED MOHIUDDIN, M. Karuna Prasad, D. Shaik Meera, Angadi Deepa N.

ABSTRACT: This study investigates the combined effects of variable thermal conductivity and temperature-dependent viscosity on the flow and heat energy transfer behaviour of a Casson nanofluid, specifically involving copper nanoparticles suspended in a water-based medium. These nanofluids are highly applicable to practical systems such as electronic cooling devices, polymer extrusion processes, and biomedical applications such as targeted drug delivery, where enhanced thermal performance of non-Newtonian fluids is crucial. The governing momentum and energy equations are expressed as a coupled set of second-order non-linear ordinary differential equations, which are then solved. These equations have been resolved using both numerical techniques (BVP5C solver in MATLAB) and analytical method. The results of both methods show strong agreement, validating the reliability of the analytical approach. Key findings reveal that incorporating copper nanofluid particles increases the effective thermal conductivity of water (base fluid) by up to 16%, resulting in a 15-20% improvement in the heat transfer rate. Additionally, temperature-dependent viscosity improves the velocity distribution by approximately 12.24% contributing to more efficient thermal transport. The novelty of this work lies in its comprehensive treatment of temperature-sensitive thermal conductivity , viscosity effects in Casson nanofluids, which are often overlooked or treated in isolation in previous studies. By integrating these parameters, the study provides a more realistic and insightful model for optimizing thermal systems that utilize non-Newtonian nanofluids.

Keywords: Viscous dissipation, variable viscosity, casson nanofluid, variable thermal conductivity.

Contents

1. Introduction

The fundamental states of matter, fluids are characterized by their capacity to deform continuously and respond dynamically to external forces. Within the broader category of non-Newtonian fluids, which display intricate nonlinear relationships between stress and strain, Casson fluids stand out due to their visco-inelastic characteristics. These fluids find extensive application across diverse industrial sectors, including polymer extrusion processes, inkjet printing technologies, and food processing operations. Contemporary research has significantly enhanced our comprehension of how Casson fluids behave across various physical conditions. The work of Mahanta and Shaw et al. [1] focused on flow characteristics across permeable stretching surfaces, whereas Kataria and Patel et al. [2] examined heat transfer mechanisms within oscillating channel geometries. The investigation by Ramana Reddy et al. [3] explored cross-diffusion phenomena alongside non-uniform heat distribution, while Awais et al. [4] concentrated on transport through porous structures. Further contributions by Animasaun et al. [5] addressed compressible flow behavior under exponentially stretching conditions with internal thermal generation, and

2020 *Mathematics Subject Classification:* 76A05.
Submitted November 11, 2025. Published February 26, 2026

Pourmehran et al. [6] studied the coupling of buoyancy forces with radiative effects. Mahanthesh et al. [7] examined the research established in the enhanced thermal capabilities of metallic nanofluids when integrated with Casson fluid mechanics.

The complex interrelationship between fluid viscosity and thermal conductivity highlights their significance across numerous scientific disciplines and engineering sectors. Although these transport properties may exhibit constancy under certain operational conditions, their fundamental characteristics undergo substantial transformation when subjected to temperature fluctuations. This temperature-dependent behavior originates primarily from thermal energy production due to internal frictional dissipation, which simultaneously modifies flow characteristics and influences thermal energy transport mechanisms. Recognizing these interdependencies is vital for process optimization across industries spanning chemical production to thermal control systems, emphasizing the necessity for continued investigation into temperature-induced variations in these critical properties, as highlighted by Abrar et al. [8]. The research conducted by Kuznetsov et al. [9] placed particular emphasis on temperature-dependent viscosity and thermal conductivity characteristics. Hassan et al. [10] established that viscosity exhibits a declining trend with rising temperature, attributable to enhanced molecular motion a crucial factor in the current analysis

Investigation into thermal transport media across various industrial applications uncovers an essential interplay between operational capability and performance optimization, as demonstrated in the work of Gbadeyan et al. [11]. Conventional heat transfer fluids, including water and mineral-based oils, serve critical functions in power production facilities, microelectronic cooling systems, and climate control technologies, however their limited thermal conductivity presents inherent performance constraints. The incorporation of nanoscale particles has transformed this field by substantially augmenting thermal conductivity, thereby overcoming the deficiencies associated with traditional media. This methodology enhances energy utilization efficiency while simultaneously creating opportunities for sophisticated applications throughout industrial sectors. With advancing technology, nanoparticle integration into thermal management systems is poised to establish new performance benchmarks and accelerate innovation in heat transfer solutions. Research by Kalteh et al. [12] demonstrated that alumina-water nanofluid suspensions exhibit superior heat conduction properties. Rasheed et al. [13] investigated the thermal enhancement capabilities of copper-based nanoparticles. The addition of copper nanoparticles amplifies convective thermal transport by improving the fluid's heat conduction characteristics. Relative to alternative metal oxide additives, copper nanoparticle dispersion within fluids produces substantial increases in the Nusselt number, a dimensionless parameter quantifying convective heat transfer efficiency. This superior performance stems from copper's inherently high thermal conductivity compared to most metal oxides. Furthermore, copper demonstrates advantageous characteristics including remarkable stability and beneficial chemical properties. The thermal storage capacity of copper nanoparticles exceeds that of silver-based alternatives. Copper-water (cu-H_2O) nanofluid systems are specifically formulated by suspending highly conductive nanoparticles within traditional base fluids to attain enhanced thermal transport characteristics. These engineered fluids demonstrate improved effective thermal conductivity, modified viscosity, and elevated convective heat transfer coefficients relative to pure carrier fluids. Experimental investigations have documented that Cu-water nanofluids can achieve heat transfer performance improvements ranging from 10–30% influenced by nanoparticle concentration and operating temperature. Copper nanoparticle incorporation yields notable thermal conductivity enhancement, resulting in 16–25% improvement in heat transfer efficiency compared to base fluids, with performance variations dependent on volumetric particle fraction and thermal boundary conditions. The integrated temperature-dependent thermal conductivity into magnetohydrodynamic boundary layer flow analysis to capture realistic heat transfer behavior in thermally sensitive fluids. Their mathematical model incorporated a linear temperature dependence for the fluid's thermal conductivity.

The research of Mabood et al. [14] examined how temperature-dependent viscosity affects magnetohydrodynamic nanofluid transport across nonlinearly stretching surfaces. Their findings revealed that temperature variations substantially alter fluid viscosity, consequently affecting both velocity distribution and thermal boundary layer development. Shehzad et al. [15] investigated the influence of variable viscosity on magnetohydrodynamic nanofluid motion over nonlinear stretching geometries. Their analysis demonstrated significant temperature-induced viscosity modifications, impacting both momentum and

thermal boundary layer characteristics. Additionally, their work incorporated temperature-dependent thermal conductivity within the MHD boundary layer framework to accurately represent heat transfer processes in thermally responsive fluids. Idowu et al. [16], analytical approach implemented a linear temperature relationship for the fluid's thermal conductivity parameter.

The investigations conducted by Kim et al. [17] and Bahiraei et al. [18] focused on nanoparticle transport mechanisms and spatial concentration distributions, respectively. Comparative analysis by Samrat et al. [19] established that silver nanoparticles demonstrate superior thermal extraction capabilities compared to copper and iron alternatives, whereas Rawi et al. [20] employed the Keller Box computational technique for copper-based nanofluid analysis. These research outcomes hold significant relevance for thermal engineering implementations, including nuclear reactor thermal management, petroleum recovery enhancement processes solar energy collection systems, and miniaturized heat exchange devices. Such applications demand precise thermal performance regulation within restrictive geometric configurations, where Non-Newtonian fluids augmented with nanoparticles provide considerable advantages. The work of Aziz et al. [21] validated the applicability of metallic nanofluids across biomedical technologies, solar energy systems, and porous medium applications.

Despite considerable advancements in nanofluid flow modeling. The synergistic effects of radiative thermal transport combined with concurrent variations in both viscosity and thermal conductivity remain insufficiently investigated within comprehensive analytical frameworks. Through the integration of copper nanoparticles, Casson fluid rheological behavior and sophisticated thermal modelling techniques present investigation contributing to the development of the research literature, thereby advancing the development of next-generation thermal fluid technologies.

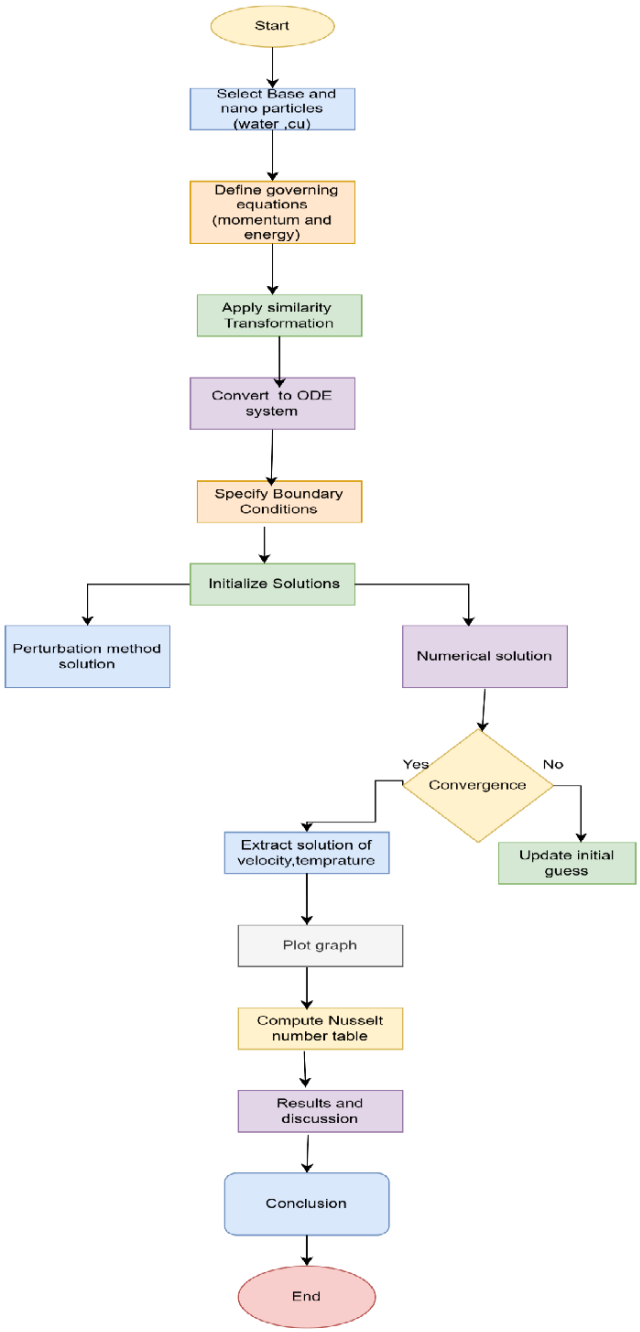

Figure 1: Computational workflow for Casson nanofluid analysis with variable viscosity and thermal conductivity

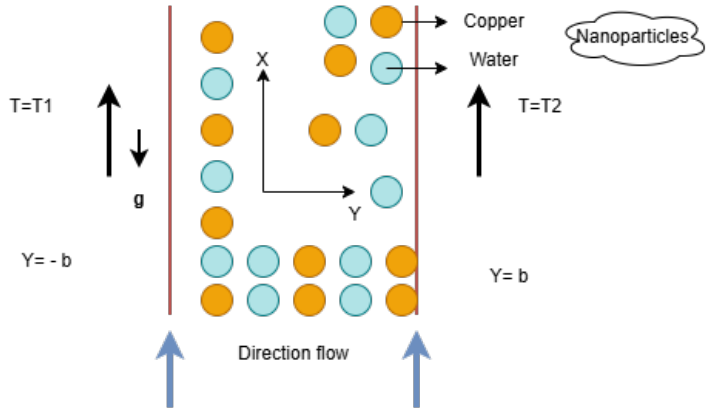

Figure 2: Physical Configuration

2. Mathematical Model of the Problem

The exploration of nanofluids flow behavior reveals a complex interplay of geometric factors and the distinctive properties that these advanced fluids exhibit. By employing a dual-axis approach, with vertical movement represented by the x-axis and perpendicular dimensions by the y-axis, this study effectively illustrates how these elements influence both heat transfer and fluid mechanics. The insights gained not only enhance our understanding of nanofluid dynamics but also lay a solid foundation for future research and potential applications across various industries. As we continue to unravel the intricacies of nanofluids, their promising capabilities hold significant implications for improving thermal management systems and revolutionizing fluid transport technologies. The temperature of the left and right walls is kept constant. The buoyancy forces cause the fluid to ascend within the channel. The x no-slip boundary condition is satisfied by the parallel plates for velocity. Along the x-axis, the plates are considered infinitely long and the physical variables remain unchanged in this direction.

The Vector form of momentum and energy equations are

$$\left(1+\frac{1}{\beta}\right)\nabla\cdot(\mu_{nf}\nabla\vec{U_1})+(\rho\beta)_{nf}g(T-T_0)-\frac{\mu_{nf}}{K}\vec{U_1}-\nabla p=0 \tag{2.1}$$

$$\nabla\cdot(k_{nf}\nabla\vec{T})+\left(1+\frac{1}{\beta}\right)\mu_{nf}\left|\vec{U_1}\right|^2+\frac{\mu_{nf}}{K}\left|\vec{U_1}\right|^2=0 \tag{2.2}$$

The momentum and energy equations are given by (Umavathi et.al [22])

$$\left(1+\frac{1}{\beta}\right)\frac{d}{dY}\left(\mu_{nf}\frac{dU_1}{dY}\right)+(\rho\beta)_{nf}g(T-T_0)-\frac{\mu_{nf}}{K}U_1-\frac{\partial p}{\partial X}=0 \tag{2.3}$$

$$\frac{d}{dY}\left(K_{nf}\frac{dT}{dY}\right)+\left(1+\frac{1}{\beta}\right)\mu_{nf}\left(\frac{dU_1}{dY}\right)^2+\frac{\mu_{nf}}{K}U_1^2=0 \tag{2.4}$$

Where U_1 denotes the velocity, T is the temperature and ρ is the density, μ is viscosity, k is thermal conductivity and β_t is the coefficient of thermal expansion, g represents the acceleration due to gravity, β is the Casson parameter and p denotes the pressure, Thermal expansion coefficient of the base fluid and β_s is Thermal expansion coefficient of solid nanoparticles β_f (Buongiorno et al. [23])

The velocity and temperature field's boundary conditions are

$$U_1 = 0,\ T = T_1 \text{ at } Y = -b \tag{2.5}$$

$$U_1 = 0,\ T = T_2 \text{ at } Y = b \tag{2.6}$$

The fundamental thermophysical characteristics of the nano fluid are (Rasheed et al. [13])

$$(\rho\beta)_{nf} = (1-\phi)(\rho\beta)_f + \phi(\rho\beta)_s, \quad \sigma_{nf} = \sigma_f \left[\frac{1 + 3\phi\left(\frac{\sigma_s}{\sigma_f} - 1\right)}{\left(\frac{\sigma_s}{\sigma_f} + 2\right) - \left(\frac{\sigma_s}{\sigma_f} - 1\right)\phi} \right], \quad \mu_{nf} = \frac{\mu_f}{(1-\phi)^{2.5}},$$
$$\rho_{nf} = (1-\phi)\rho_f + \phi\rho_s, \qquad \kappa_{nf} = \kappa_f \left(\frac{\kappa_s + 2\kappa_f - 2\phi(\kappa_f - \kappa_s)}{\kappa_s + 2\kappa_f + \phi(\kappa_f - \kappa_s)} \right) \tag{2.7}$$

Table 1: Thermophysical properties of nanofluids and base fluids

Model	$\rho\,(\mathrm{kg/m^3})$	$k\,(\mathrm{Wm^{-1}K^{-1}})$	$\beta_t \times 10^{-5}\,(\mathrm{K^{-1}})$	$\sigma\,(\mathrm{m^{-2}})$
H_2O	997.1	0.613	21	5.5×10^{-6}
Cu	8933	401	1.67	5.96×10^{7}
Ag	10500	429	1.89	6.3×10^{7}
Al_2O_3	3970	40	0.85	6.68×10^{-10}
TiO_2	4250	8.9528	0.9	2.38×10^{6}
Fe_3O_4	5180	9.7	0.5	2.5×10^{4}
$C_2H_6O_2$	1.115	0.1490	6.5	6.1×10^{-6}

The volumetric expansion of solutal water is $\beta_c = 298.2$ and copper is $Cu = 3.05 \times 10^6\,(m^2/h)$ (Bhuvaneshwari et al. [24]), As the temperature varies, it is assumed that the viscosity of the fluid varies (Umavathi et al. [22]).

$$\mu = \mu_0\, e^{-a(T-T_0)} \tag{2.8}$$

Liquids such as benzene, crude oil, and water generally exhibit a positive Joule–Thomson coefficient, indicating cooling upon expansion. In contrast, gases like helium and methane may display negative values under certain conditions, such as in atmospheric air, resulting in heating during expansion.$a$is the empirical constant for dynamic viscosity and range is 0.001-0.001 is observed by (Maziar Dehghan et al. [25]) the fluid's thermal conductivity is expected to be

$$K \;=\; K_0\, e^{-b(T\;-\;T_0)} \tag{2.9}$$

nanofluids containing relatively small nanoparticle concentrations (1–5 voł

The following dimensionless parameters can be used to formulate Eqs. (3)-(4):

$$u^* = \frac{U_1}{\bar{u}}, \quad y^* = \frac{Y}{b}, \quad \mathrm{Gr}_{T1} = \frac{g\,\beta_T\,b^3\,\Delta T}{\bar{u}^2}, \quad P = \frac{b^2}{\mu_0 \bar{u}}\frac{\partial p}{\partial X}$$
$$GR_{T1} = \frac{Gr_{T1}}{Re}, \quad Br_t = \frac{\mu_0 \bar{u}^2}{k_0 \Delta T_1}, \quad \mu_{nf} = \frac{\mu_f}{(1-\phi)^{2.5}}, \quad \theta^* = \frac{T - T_0}{\Delta T_1}, \quad \sigma = \frac{b}{\sqrt{k}} \tag{2.10}$$

where Re is the Reynolds number, Gr_{T1} is the thermal Grashof number, GR_{T1} is the modified thermal Grashof number, this Heat transformation yields the non-dimensional form of the governing equations, which facilitates the derivation of Equations (2.3)-(2.4).

$$\frac{d^2u}{dy^2} - b_{v1}\frac{d\theta}{dy}\frac{du}{dy} + (1 + b_{v1}\theta)\,(F_1 GR_{T1}\theta - F_2 P) - F_3\sigma^2 u = 0 \tag{2.11}$$

$$\begin{aligned} &\frac{d^2\theta}{dy^2} - b_{k1}\left(\frac{d\theta}{dy}\right)^2 + Br_1F_6\left(\frac{du}{dy}\right)^2 - Br_1F_6(b_{v1} - b_{k1})\theta\left(\frac{du}{dy}\right)^2 \\ &-Br_1F_6b_{v1}b_{k1}\theta^2\left(\frac{du}{dy}\right)^2 + Br_1F_7\sigma^2u^2 - Br_1F_7(b_{v1} - b_{k1})\sigma^2u^2\theta \\ &-Br_1F_7b_{v1}b_{k1}\sigma^2u^2\theta^2 = 0 \end{aligned} \tag{2.12}$$

Here u, θ, y and p are dimensionless velocity, temperature, coordinate axis, and pressure. $b_{v1} = a\,\Delta\,T_1$ is the variable viscosity parameter, then $b_{k1} = b\,\Delta\,T_1$ is the variable thermal conductivity parameter, m is the wall temperature ratio, Br_1 is the Brinkman number.
The nanofluids constant parameters are

$$\begin{aligned} &A_1 = (1-\phi)^{2.5},\ A_2 = \frac{1}{\left(1+\frac{1}{\beta}\right)},\ A_3 = (1-\phi) + \phi\frac{(\rho\beta)_s}{(\rho\beta)_f}, \\ &F_1 = A_1A_2A_3,\ F_2 = A_1A_2,\ F_3 = A_2,\ F_4 = \frac{\kappa_{os}+2\kappa_{of}-2\phi(\kappa_{of}-\kappa_{os})}{\kappa_{os}+2\kappa_{of}+\phi(\kappa_{of}-\kappa_{os})}, \\ &F_5 = \frac{1}{A_1A_2}, F_6 = \frac{F_5}{F_4}, F_7 = \frac{1}{A_1F_4} \end{aligned} \tag{2.13}$$

The boundary conditions are

$$u = 0 \text{ at } y = \pm 1 \tag{2.14}$$

$$\theta = 1 + m \text{ at } y = -1, \quad \theta = 1 \text{ at } y = 1 \tag{2.15}$$

Solving Eqs. (2.11)-(2.12) Analytically is difficult as they are coupled systems of nonlinear equations. It is possible to find approximate analytical solutions by using the regular perturbation approach. Analytical solutions are easier to find for Eqs. (2.11) and (2.12).

$$u = u_0 + Bru_1 \tag{2.16}$$

$$\theta = \theta_0 + Br\theta_1 \tag{2.17}$$

The zeroth order equations

$$\frac{d^2u_0}{dy^2} - b_{v1}\frac{d\theta_0}{dy}\frac{du_0}{dy} + F_1GR_{T1}\theta_0 + F_1b_{v1}GR_{T1}{\theta_0}^2 - F_2P - F_2b_{v1}P\theta_0 - F_3\sigma^2u = 0 \tag{2.18}$$

$$\frac{d^2\theta_0}{dy^2} - b_{k1}\left(\frac{d\theta_0}{dy}\right)^2 = 0 \tag{2.19}$$

The boundary conditions are

$$u_0 = 0 \quad \text{at} \quad y = \pm 1 \tag{2.20}$$

$$\theta_0 = 1 + m, \quad \text{at} \quad y = -1, \theta_0 = 1 \quad \text{at} \quad y = 1 \tag{2.21}$$

First-order equations

$$\frac{d^2u_1}{dy^2} - b_{v1}\frac{du_0}{dy}\frac{d\theta_1}{dy} - b_{v1}\frac{du_1}{dy}\frac{d\theta_1}{dy} + F_1b_{v1}GR_{T1}\theta_1\theta_0 + F_1GR_{T1}\theta_1 - F_3b_{v1}\theta_1P - F_3\sigma^2u_1 = 0 \tag{2.22}$$

$$\begin{aligned} \frac{d^2\theta_1}{dy^2} - 2b_{k1}\frac{d\theta_0}{dy}\frac{d\theta_1}{dy} + F_4b_{v1}\left(\frac{du_0}{dy}\right)^2 - F_4(b_{v1}-b_{k1})\theta_0\left(\frac{du_0}{dy}\right)^2 - F_4b_{v1}b_{k1}\theta_0^2\left(\frac{du_0}{dy}\right)^2 \\ -F_5(b_{v1}-b_{k1})u_0^2\sigma^2\theta_0 - F_5b_{v1}b_{k1}u_0^2\sigma^2\theta_0^2 + F_6u_0^2\sigma^2 = 0 \end{aligned} \tag{2.23}$$

The boundary conditions are

$$u_1 = 0 \quad \text{at} \quad y = \pm 1 \tag{2.24}$$

$$\theta_1 = 1 + m \quad \text{at} \quad y = -1, \quad \theta_1 = 1 \quad \text{at} \quad y = 1 \tag{2.25}$$

The coupled and nonlinear Equations (2.18)–(2.19) and (2.22)–(2.23) remain coupled and nonlinear even after applying the initial perturbation method. Therefore, the perturbation technique is applied

once more, treating the variable thermal conductivity parameter as the perturbation parameter. It is assumed that Equations (2.18) and (2.19) admit the following approximate solutions.

$$u_0 = u_{00} + b_{k1}u_{01} \tag{2.26}$$

$$\theta_0 = \theta_{00} + b_{k1}\theta_{01} \tag{2.27}$$

Eqs. (2.27)-(2.28) are substituted in Eqs. (2.19)-(2.20) and then we equate the constants terms, and the Coefficients of b_k to get the following equations.

The zeroth order equations

$$\frac{d^2u_{00}}{dy^2} - b_{v1}\frac{d\theta_{00}}{dy}\frac{du_{00}}{dy} + (1 + b_{v1}\theta_{00})\,(F_1GR_{T1}\theta_{00} - F_2P) - F_3\sigma^2u_{00} = 0 \tag{2.28}$$

$$\frac{d^2\theta_{00}}{dy^2} = 0 \tag{2.29}$$

First-order equations

$$\frac{d^2u_{01}}{dy^2} - b_{v1}\frac{d\theta_{00}}{dy}\frac{du_{01}}{dy} - b_{v1}\frac{d\theta_1}{dy}\frac{du_{00}}{dy} + F_1\,(1 + b_{v1}\theta)\,GR_{T1}\theta_{01} + b_{v1}\theta_{01}\,(F_1GR_{T1}\theta_{00} - F_3P) - F_3\sigma^2u_{01} = 0 \tag{2.30}$$

$$\frac{d^2\theta_{01}}{dy^2} - \left(\frac{d\theta_{00}}{dy}\right)^2 = 0 \tag{2.31}$$

The boundary conditions are

$$u_{00} = 0 \text{ at } y = \pm 1,\ \theta_{00} = 1 + m \quad \text{at} \quad y = -1,\ \theta_{00} = 1 \quad \text{at} \quad y = 1 \tag{2.32}$$

$$u_{01} = 0 \text{ at } y = \pm 1,\ \theta_{01} = 0 \quad \text{at } y = \pm 1 \tag{2.33}$$

Solving Eqs. (2.28), (2.29), (2.30) and (2.31) yields

$$u_{00} = c_5e^{\alpha_1 y} + c_6e^{\alpha_2 y} + h_1y^2 + h_2y + h_3 \tag{2.34}$$

$$\theta_{00} = c_1y + c_2 \tag{2.35}$$

$$\theta_{01} = l_1y^2 + c_3y + c_4 \tag{2.36}$$

$$u_{01} = c_7e^{\alpha_3 y} + c_8e^{\alpha_4 y} + d_1ye^{\alpha_1 y} + d_2ye^{\alpha_2 y} + d_3e^{\alpha_1 y} + d_4e^{\alpha_2 y} + d_5y^3 + d_6y^2 + d_7y + d_8 \tag{2.37}$$

where

$$q_1 = -F_1c_1^2b_{v1}GR_{T1} \quad , \ q_2 = -F_1c_1GR_{T1} - 2F_1c_1c_2b_{v1}GR_{T1} + F_2c_1b_{v1}P \quad ,$$
$$q_3 = -F_1c_2GR_{T1} - F_1c_2^2GR_{T1} + F_2c_2b_{v1}P + F_3P$$

$$h_1 = \frac{-q_1}{g_1} \quad , \ h_2 = \frac{2m_1q_1}{g_1^2} - \frac{q_2}{g_1} \quad , \ h_3 = \frac{-2q_1}{{g_1}^2} - \frac{2m_1q_1}{{g_1}^3} + \frac{m_1q_2}{{g_1}^2} - \frac{-q_1}{g_3}$$

$$g_1 = A_2 \quad , \ g_2 = 2\alpha_1 - m_1 \quad g_3 = \alpha_1^2 - m_1\alpha_1 - g_1 \quad , \ g_4 = 2\alpha_2 - m_1$$

$$g_5 = \alpha_2^2 - m_1\alpha_2 - g_1 \quad , \; g_6 = \alpha_1^2 - m_1\alpha_1 - g_1 \quad , \; g_7 = \alpha_2^2 - m_1\alpha_2 - g_1$$

$$w_1 = 2c_5 b_{v1} l_1 \alpha_1 \quad , \; w_2 = 2c_6 b_{v1} l_1 \alpha_2 \quad , \; w_3 = b_{v1} c_3 c_5 \alpha_1 \quad , \; w_4 = b_{v1} c_3 c_6 \alpha_2$$

$$w_5 = -2F_1 c_1 b_{v1} G R_{T1} l_1 \quad , w_6 = 4b_{v1} l_1 h_1 - F_1 G R_{T1} l_1 - 2F_1 c_1 c_3 b_{v1} G R_{T1} - 2F_1 c_2 b_{v1} G R_{T1} l_1 + F_2 b_{v1} P l_1,$$

$$w_7 = 2b_{v1} l_1 h_2 + 2b_{v1} c_3 h_1 - F_1 c_1 c_3 G R_{T1} - 2F_1 c_1 c_4 b_{v1} G R_{T1} - 2F_1 c_1 c_3 b_{v1} - F_2 c_3 b_{v1} P$$

$$w_8 = b_{v1} c_3 h_2 - F_1 c_4 G R_{T1} - 2F_1 c_2 c_4 b_{v1} G R_{T1} + F_2 b_{v1} P$$

$$d_1 = \frac{w_1}{g_3}, \quad d_2 = \frac{w_2}{g_5}, \quad d_3 = \frac{w_1 g_2}{g_3^2} + \frac{w_3}{g_6}, \quad d_4 = \frac{w_2 g_4}{g_5^2} + \frac{w_4}{g_7}, \quad d_5 = \frac{-w_5}{g_1},$$

$$d_6 = \frac{3m_1 w_5}{g_1^2} - \frac{w_6}{g_1}, \; d_7 = \frac{6w_5}{g_1^2} - \frac{6m_1 w_5}{g_1^3} + \frac{2m_1 w_6}{g_1^2} - \frac{w_7}{g_1} \quad , \; d_8 = \frac{12m_1 w_5}{g_1^3} + \frac{6m_1^2 w_5}{g_1^4} - \frac{2w_6}{g_1^2} - \frac{2w_6 m_1}{g_1^3} + \frac{w_7 m_1}{g_1^2} - \frac{w_8}{g_1}$$

where

$$c_1 = \frac{-m}{2}, \quad c_2 = \frac{2+m}{2}, \quad c_3 = 0, \quad c_4 = -l_1$$

$$c_5 = \frac{1}{e^{(\alpha_1-\alpha_2)} - e^{(-\alpha_1-\alpha_2)}} \left(h_1(e^{-\alpha_2} - e^{\alpha_2}) + h_2(e^{-\alpha_2} + e^{\alpha_2}) + h_3(e^{-\alpha_2} - e^{\alpha_2}) \right)$$

$$c_6 = \frac{-1}{e^{\alpha_2}} \left[c_5 e^{\alpha_1} + h_1 + h_2 + h_3 \right]$$

$$c_7 = \frac{-1}{e^{\alpha_3}} \left[c_8 e^{\alpha_4} + d_1 e^{\alpha_1} + d_2 e^{\alpha_2} + d_3 e^{\alpha_3} + d_4 e^{\alpha_4} + d_5 + d_6 + d_7 + d_8 \right]$$

$$\begin{aligned} c_8 = \frac{-1}{e^{-\alpha_3+\alpha_4} - e^{\alpha_3-\alpha_4}} \Big[& d_1\big(e^{\alpha_1-\alpha_3} + e^{-\alpha_1-\alpha_3}\big) + d_2\big(e^{\alpha_2-\alpha_3} - e^{-\alpha_2-\alpha_3}\big) \\ & + d_3\big(e^{\alpha_1-\alpha_3} - e^{-\alpha_1-\alpha_3}\big) + d_4\big(e^{\alpha_2-\alpha_3} - e^{-\alpha_2-\alpha_3}\big) \\ & + d_5\big(e^{-\alpha_3} + e^{\alpha_3}\big) + d_6\big(e^{-\alpha_3} - e^{\alpha_3}\big) \\ & + d_7\big(e^{-\alpha_3} + e^{\alpha_3}\big) + d_8\big(e^{-\alpha_3} - e^{\alpha_3}\big) \Big] \end{aligned} \tag{2.38}$$

This research examines the behavior of Casson nanofluid flow within a vertical channel through both analytical and computational approaches, incorporating temperature-dependent viscosity and thermal conductivity properties. The numerical analysis employs MATLAB's BVP5C solver for visualization and solution processing. The investigation quantifies skin friction coefficients and Nusselt numbers across various governing parameters, presenting these findings in tabular format. The study considers the temperature dependency of both viscosity and thermal conductivity to better characterize the fluid flow behavior, with results presented for specific parameter values

3. Graphs and Tables

$m = -1, \; b_{v1} = 0.2, \; b_{k1} = 0.2, \; P = 0.2, \; GR_{T1} = 10, \; Br_1 = 0.01, \; \sigma = 2, \phi = 0.01, \; \beta = 0.5$

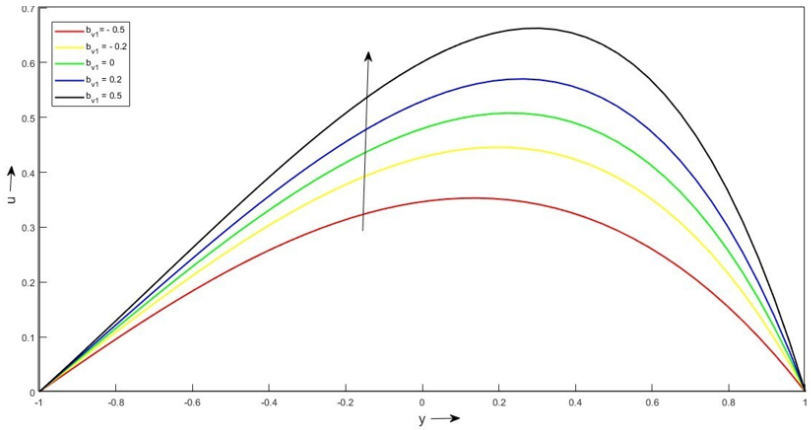

Figure 3: Velocity profile for b_{v1}

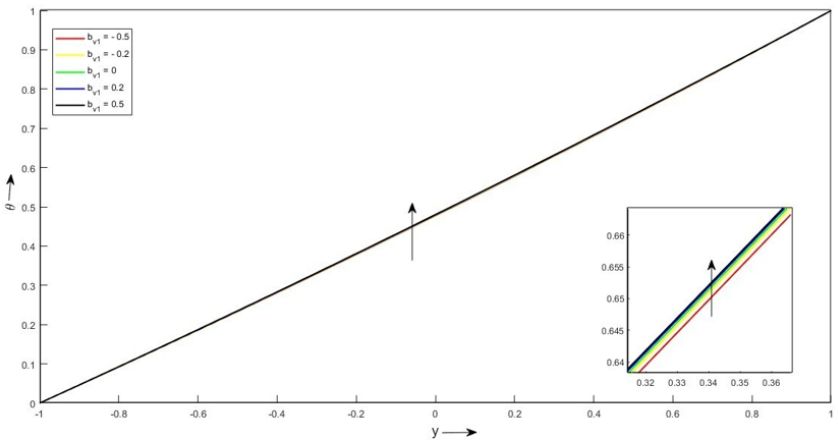

Figure 4: Temperature profile for b_{v1}

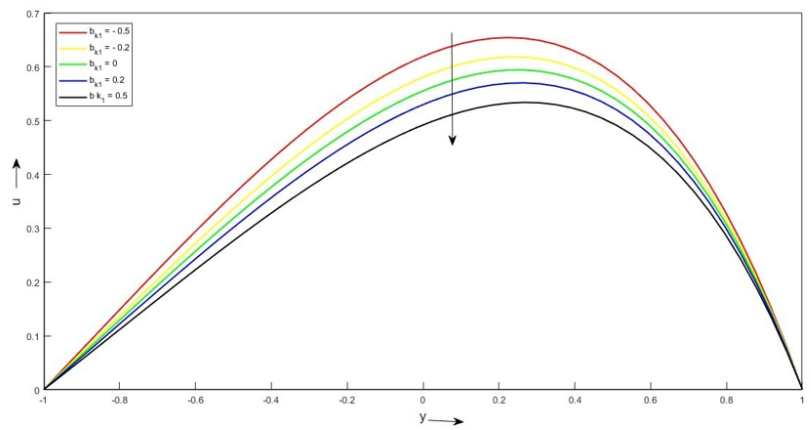

Figure 5: Velocity profile for b_{k1}

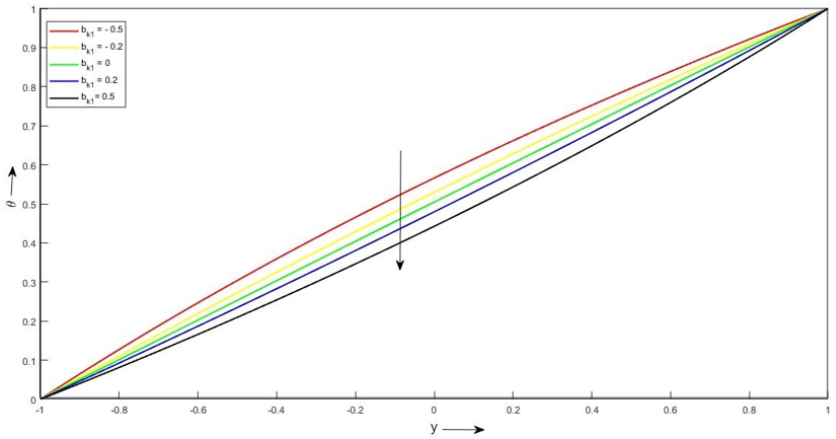

Figure 6: Temperature profile for b_{k1}

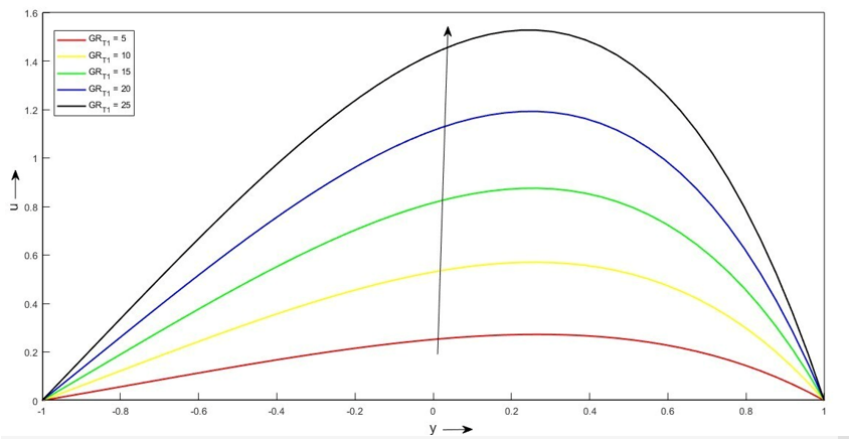

Figure 7: Velocity profile for GR_{T1}

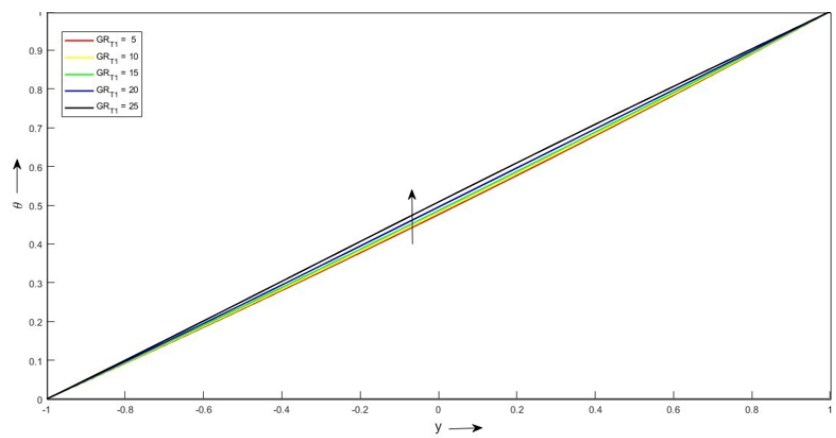

Figure 8: Temperature profile for GR_{T1}

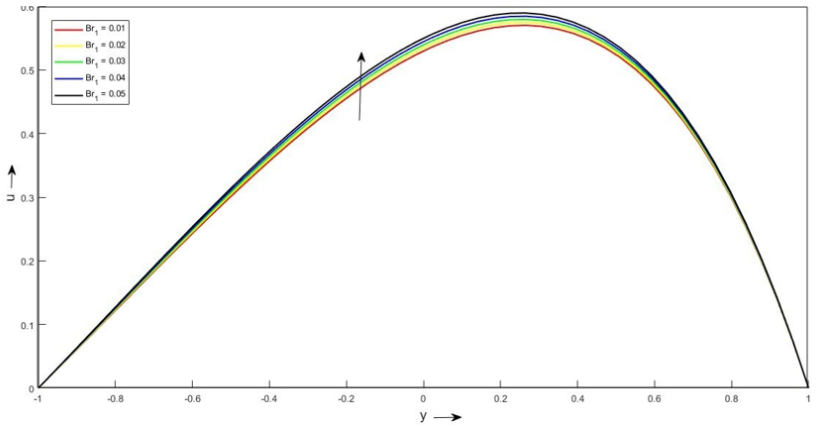

Figure 9: Velocity profile for B_{r1}

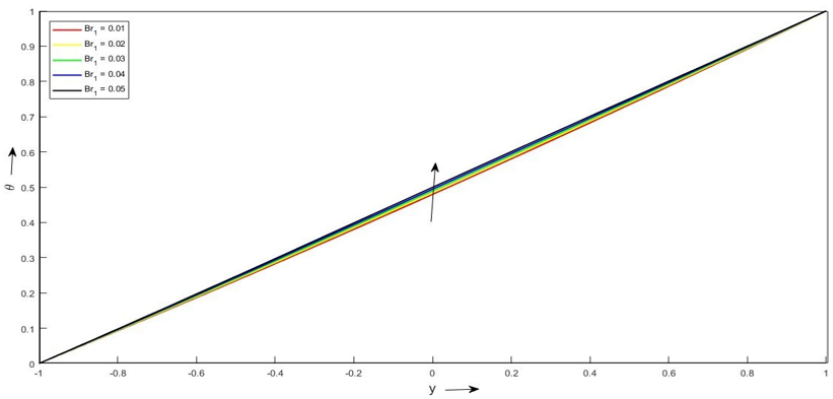

Figure 10: Temperature profile for B_{r1}

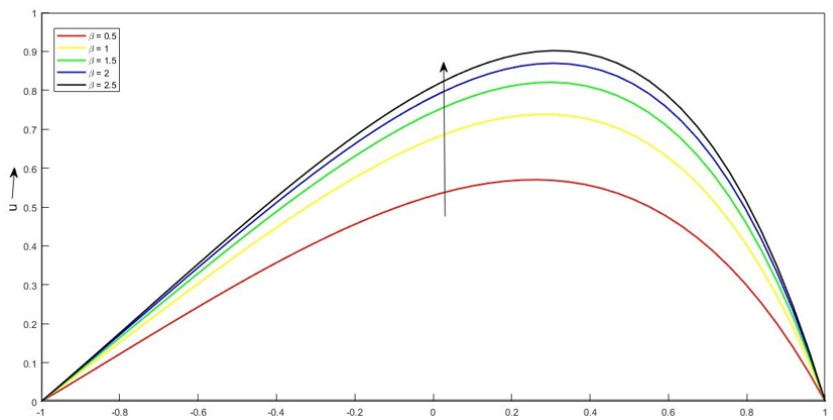

Figure 11: Velocity profile for β

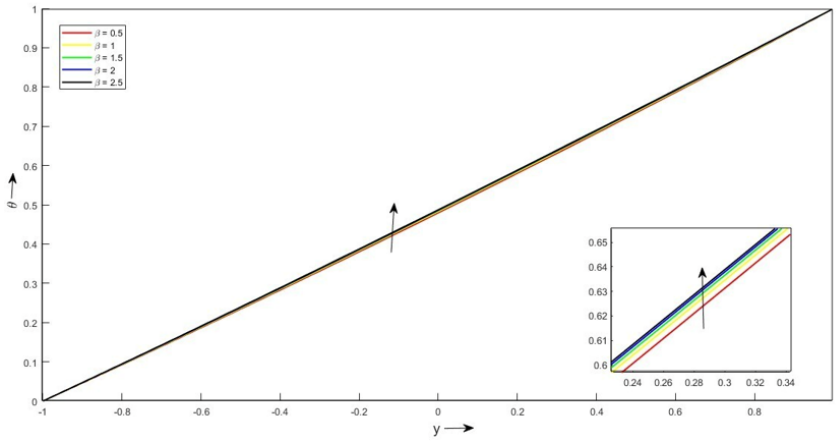

Figure 12: Temperature profile for β

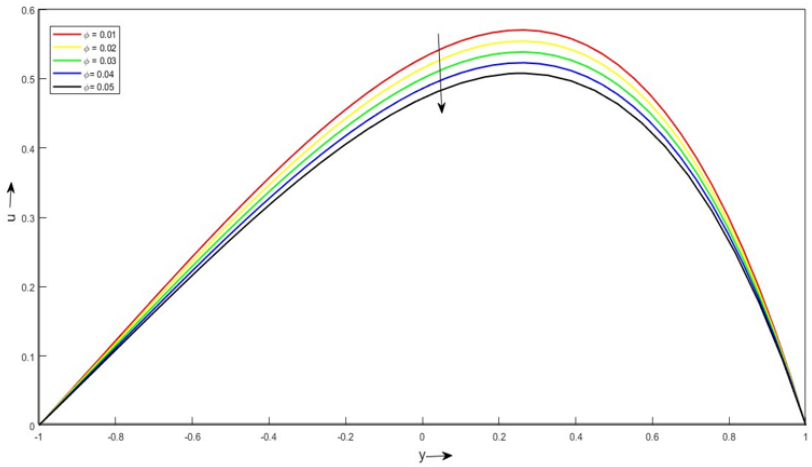

Figure 13: Velocity profile for ϕ

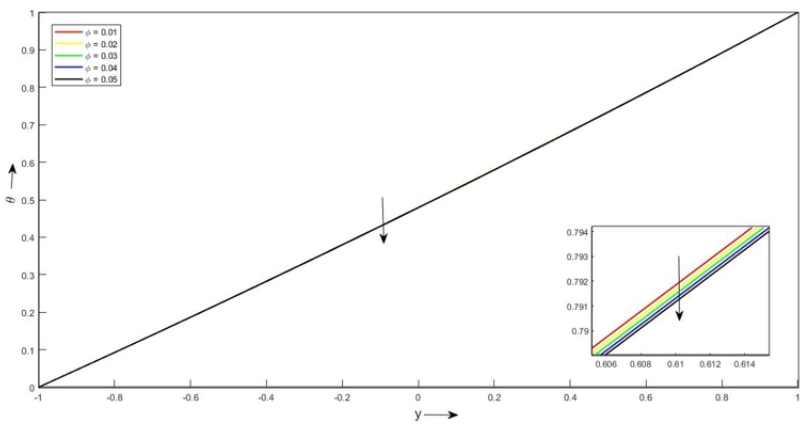

Figure 14: Temperature profile for ϕ

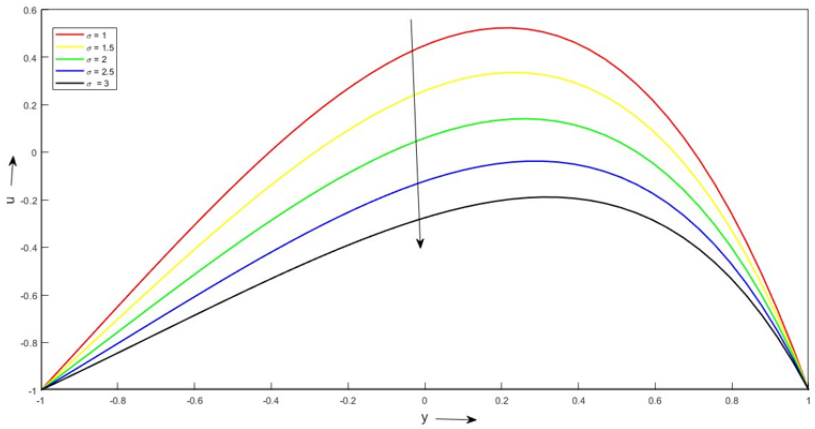

Figure 15: Velocity profile for σ

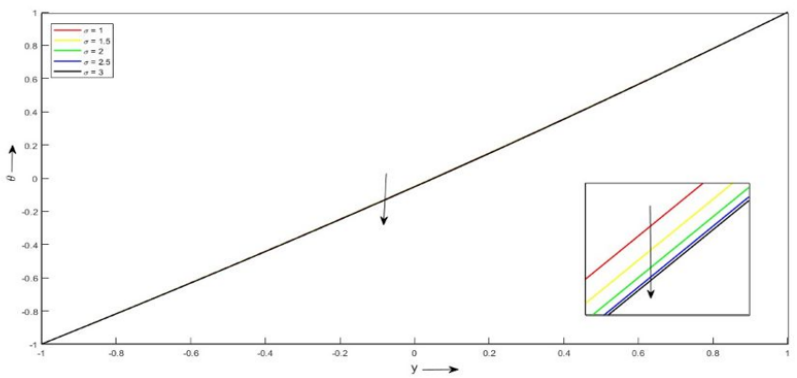

Figure 16: Temperature profile for σ

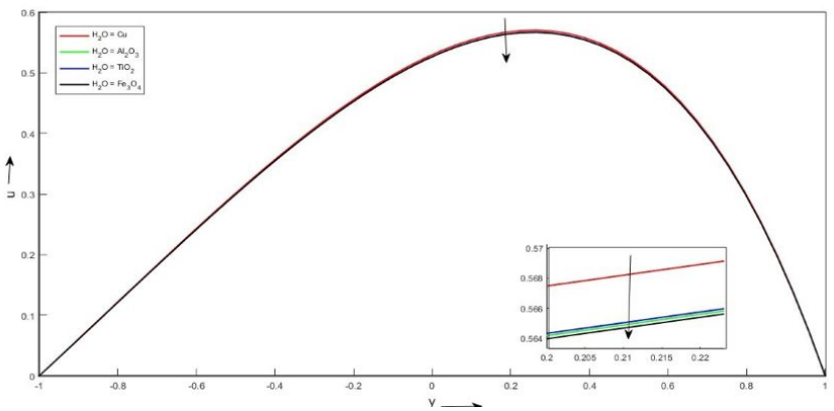

Figure 17: Velocity profile for water-based Nano fluids

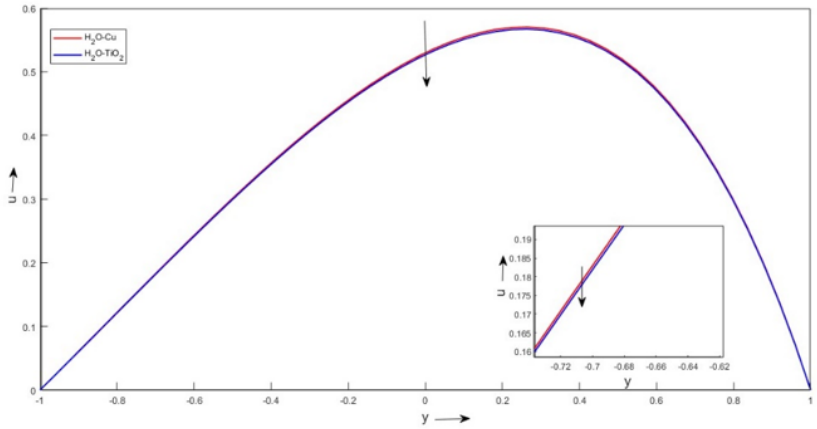

Figure 18: Velocity profile for water-based Nano fluids

4. Tables

$m = -1,\ b_{v1} = 0.2,\ b_{k1} = 0.2,\ P = 0.2,\ GR_{T1} = 10,\ Br_1 = 0.01,\ \sigma = 2, \phi = 0.01,\ \beta = 0.5$

Table 2: Comparison of numerical and analytical solutions for temperature and velocity

$Br_1 = 0$						
y	Umavathi et al. [22] $\sigma = \alpha = n = 0$ $Gr_{T1} = 1,\ Gr_C = 0$		Bhuvaneshwari et al. [24] $\phi = \sigma = n = 0,\ Gr_{T1} = 1,\ Gr_C = 0$		Present work $\phi = \sigma = 0,\ Gr_{T1} = 1$	
	Velocity	Temperature	Velocity	Temperature	Velocity	Temperature
-1.0	0.0000000	0.0000000	0.0000000	0.0000000	0.0000000	0.0000000
-0.8	0.0287189	0.0914675	0.0287189	0.0914675	0.0287188	0.0914676
-0.6	0.0624231	0.1846390	0.0624231	0.1846390	0.0624229	0.1846390
-0.4	0.0973984	0.2795780	0.0973984	0.2795780	0.0973980	0.2795790
-0.2	0.1296450	0.3763550	0.1296450	0.3763550	0.1296440	0.3763550
0.0	0.1548550	0.4750410	0.1548550	0.4750410	0.1548540	0.4750410
0.2	0.1683920	0.5757150	0.1683920	0.5757150	0.1683910	0.5757150
0.4	0.1652620	0.6784570	0.1652620	0.6784570	0.1652620	0.6784570
0.6	0.1400890	0.7833570	0.1400890	0.7833570	0.1400890	0.7833560
0.8	0.0870818	0.8905050	0.0870818	0.8905050	0.0870816	0.8905050
1.0	0.0000000	1.0000000	0.0000000	1.0000000	0.0000000	1.0000000

$Br_1 = 0.01$						
y	Umavathi et al. [22] $\sigma = \alpha = n = 0$ $Gr_{T1} = 1,\ Gr_C = 0$		Bhuvaneshwari et al. [24] $\phi = \sigma = n = 0,\ Gr_{T1} = 1,\ Gr_C = 0$		Present work $\phi = \sigma = 0,\ Gr_{T1} = 1$	
	Velocity	Temperature	Velocity	Temperature	Velocity	Temperature
-1.0	0.0000000	0.0000000	0.0000000	0.0000000	0.0000000	0.0000000
-0.8	0.0287345	0.0915082	0.0287345	0.0915082	0.0287345	0.0915083
-0.6	0.0624533	0.1847120	0.0624533	0.1847120	0.0624531	0.1847120
-0.4	0.0974405	0.2796720	0.0974405	0.2796720	0.0974401	0.2796730
-0.2	0.1296950	0.3764590	0.1296900	0.3764590	0.1296950	0.3764590
0.0	0.1549090	0.4751480	0.1549090	0.4751480	0.1549080	0.4751480
0.2	0.1684450	0.5758190	0.1684450	0.5758190	0.1684440	0.5758190
0.4	0.1653090	0.6785500	0.1653090	0.6785580	0.1653090	0.6785580
0.6	0.1401250	0.7834520	0.1401250	0.7834520	0.1401250	0.7834510
0.8	0.0871014	0.8905770	0.0871014	0.8905770	0.0871012	0.8905770
1.0	0.0000000	1.0000000	0.0000000	1.0000000	0.0000000	1.0000000

5. Results and Discussion

Casson nanofluid flow in a vertical channel is analyzed using analytical and numerical techniques where the governing model incorporates a second-order ODE to capture variations in viscosity and thermal conductivity. While the analytical approach is carried out via a perturbation method, which is valid for small parameter values, numerical solutions are achieved using MATLAB's BVP5C solver [21, 22]. It is investigated how different physical characteristics affect the temperature and velocity fields as well as the rates of heat transfer. When the viscosity variation parameter b_{v1} is set to zero, representing constant viscosity, the temperature and velocity distributions lie between those corresponding to positive and negative values of b_{v1}. A reduction in b_{v1} leads to diminished viscous resistance, resulting in decreased momentum and energy transport. Conversely, increasing b_{v1} thickens the thermal boundary layer and raises fluid temperature, consistent with the findings [22,24].

1. In Figures 3 and 4 When the viscosity variation parameter b_{v1} is set to zero, representing constant viscosity, the temperature and velocity distributions lie between those corresponding to positive and negative values of b_{v1}. A reduction in b_{v1} leads to diminished viscous resistance, resulting in decreased momentum and energy transport. Conversely, increasing b_{v1} thickens the thermal boundary layer and raises fluid temperature, consistent with the findings of [22,24].

2. In Figures 5 and 6, a similar trend is observed for the thermal conductivity variation parameter b_{k1}. As b_{k1} increases, both velocity and temperature decrease, confirming the suppression of flow due to reduced heat conduction capacity.

3. Figures 7 and 8 demonstrate the variation of velocity and temperature in response to of buoyancy-assisted or opposed flow, controlled by the Grashof parameter GR_{T1}, for $GR_{T1} > 0$, velocity profiles shift towards the hot wall (right), while for $GR_{T1} < 0$, they move towards the cold wall (left), indicating the directional dependence of buoyant forces. It is evident that both temperature and velocity rise with increasing GR_{T1}, implying that thermal buoyancy significantly enhances the flow [22,24].

4. In Figures 9 and 10, The Brinkman number Br_1representing viscous dissipation effects, also has a substantial impact. As shown i increasing Br_1 raises both velocity and temperature due to elevated internal energy generation, which enhances buoyancy forces and momentum transfer [24].

Table 3: Nusselt number values and skin friction at the left and right walls

ϕ	b_{v1}	b_{k1}	Gr_{T1}	β	Br	σ	τ_1	$-\tau_2$	$-Nu_1$	$-Nu_2$
0.01							0.6071	1.5260	0.4662	0.6306
0.02							0.5896	1.4830	0.4654	0.6326
0.03							0.5724	1.4410	0.4647	0.6345
	0						0.5803	1.5760	0.4640	0.6400
	0.2						0.6071	1.5260	0.4662	0.6306
	0.4						0.6291	1.4500	0.4685	0.6188
		0					0.6444	1.5620	0.5156	0.4677
		0.2					0.6071	1.5260	0.4662	0.6306
		0.4					0.5714	1.4890	0.4231	0.8268
			5				0.2757	0.7365	0.4561	0.6565
			10				0.6071	1.5260	0.4662	0.6306
			15				0.9572	2.3360	0.4846	0.5844
				0.2			0.3813	0.8527	-0.4610	0.6446
				0.5			0.6071	1.5260	0.4662	0.6306
				0.8			0.7092	1.9130	0.4688	0.6232
					0.01		0.6071	1.5260	0.4662	0.6306
					0.02		0.3849	0.8565	0.4690	0.6245
					0.03		0.3887	0.8604	0.4774	0.6039
						0	0.5084	0.9898	0.4632	0.6401
						1	0.4703	0.9495	0.4625	0.6414
						2	0.6071	1.5260	0.4662	0.6306

5. Figures 11 and 12, β depicts the effects of fluid on velocity and temperature distributions. As β increases, these profiles decrease, indicating that Casson fluid consumes solute species and thereby suppress transport phenomena. we see that there is an acceleration of flow temperatures with higher values of β.

6. In Figures 13 and 14 The inclusion of nanoparticles significantly affects the velocity field as the nanoparticle volume fraction (ϕ) increases, the velocity decreases slightly, especially near the channel walls. This behavior is due to the increased effective viscosity of the nanofluid, which resists flow and dampens velocity. However, near the channel center, the velocity gradient remains steeper, suggesting the presence of a boundary layer effect. Where higher thermal conductivity and nanoparticle density significantly alter the flow behavior.

7. In Figures 15 and 16, It is observed that as the porous parameter σ increases, both velocity and temperature decrease, confirming the suppression of flow due to reduced heat conduction capacity

8. Figures 17 discusses the optimal velocity for copper and water-based nanofluids followed by a Al_2O_3, Fe_3O_4 and TiO_2. This trend can be linked to the density and thermal conductivity of nanoparticles. Silver nanoparticles, having higher thermal conductivity, enhance the thermal diffusion, which in turn supports higher velocity due to reduced thermal boundary layer thickness.

9. In Figure 18 The temperature difference between the two walls creates thermal gradients that improve heat transfer and influences buoyancy forces in natural convection. Water exhibits a heat transfer rate of 3%. Based on the comparative analysis of heat transfer coefficients between TiO_2 nanofluid, Cu nanofluid and water, we conclude that the nanofluids yield superior heat transfer performance.

10. Incorporating copper nanoparticles markedly improves the effective thermal conductivity of the base fluid, using the Maxwell-Garnett model (the Maxwell-Garnett model is a theoretical model used to estimate the effective macroscopic properties, like thermal conductivity, dielectric constant, or magnetic permeability, of composite materials, particularly nanofluids and heterogeneous mixtures).It is widely used in physics, materials science, and engineering , it was found that a nanoparticle volume fraction of 5% leads to an approximate 16% increase in thermal conductivity compared to pure water. This enhancement directly influences the temperature gradient across the channel, where higher thermal conductivity reduces thermal resistance, allowing faster heat propagation through the fluid.

11. Quantitatively, the maximum velocity in the case of temperature-dependent viscosity increased from 0.5079 (constant viscosity) to 0.5701 (variable viscosity). This corresponds to a 12.24% improvement in peak velocity.

12. The results indicate that the addition of copper nanoparticles enhances the effective thermal conductivity of the fluid by approximately 16%, as predicted by theoretical models such as the Maxwell–Garnett formulation. Moreover, incorporating temperature-dependent thermal conductivity generates steeper temperature gradients near the channel wall, which in turn strengthens convective heat transport.

13. The results show that the Nusselt number rises when the nanoparticle volume fraction and thermal conductivity increase, leading to about 3 to 4% rise in heat transfer. Fluids with temperature-dependent viscosity flow faster through the channel. The temperature difference between the two walls creates thermal gradients that improve heat transfer and influences buoyancy forces in natural convection.

Table 1 displays Thermophysical properties of nanofluids and base fluids, where as Table 2 presents a comparison between the numerical and analytical solutions for velocity and temperature profiles obtained by Umavathi et al. [22], Bhuvaneshwari et al. [24], and the present investigation. The results exhibit an excellent agreement among all three data sets, with differences confined to the sixth decimal place,

confirming the accuracy and stability of the present numerical approach. The velocity is found to be zero at the channel walls and maximum at the center, while the temperature increases monotonically from the cold wall to the hot wall.This close correlation demonstrates the reliability of the proposed model for simulating the flow and thermal behaviour of nanofluids.

6. Skin Friction and Nusselt Number Analysis

Table 3 shows that increasing nanoparticle loading (ϕ) weakens convection, reducing Nu on the left wall and increasing it on the right wall, while slightly redistributing wall shear. Higher particle concentration increases effective viscosity, suppressing flow mobility near the hot wall but the redistributed velocity profile strengthens the gradient at the right wall. Strengthening viscosity–temperature coupling (b_v) boosts left-wall shear and Nu but reduces the same on the right wall. When viscosity decreases more strongly with temperature, hotter regions become more fluid-like, increasing shear and heat transfer on the hot side, meanwhile, the colder wall experiences thickened velocity boundary layers, reducing shear and Nu . Enhancing conductivity (b_k) suppresses Nu at the left wall and increases Nu at the right wall, and lowers both left and right wall shear. Higher thermal conductivity spreads heat more uniformly, reducing temperature gradients at the left wall, but the energy redistributed towards the right wall increases Nu . The smoother overall velocity gradient reduces τ_1, andτ_2, Increasing GR_{T1} markedly elevates Nu_1 and Nu_2 but lowers τ_1, and τ_2,. Stronger buoyancy enhances upward motion and convective heat transfer, increasing Nu on both walls. However, buoyancy-driven flow reduces near-wall shear stress at both walls, causing τ_1, and τ_2, to decrease. As the Casson parameter β increases, the fluid becomes more Newtonian Nu rises at the left wall and falls at the right wall, whereas τ_1, and τ_2, increase at both the walls. Higher β reduces yield stress, improving flow near the hot wall, but the right-wall temperature gradient weakens. Lower yield stress also increases velocity gradients at both walls, raising τ_1, and τ_2,. Viscous dissipation Br_1 diminishes Nu at the left wall and increases it at the right wall, while τ_1, and τ_2, decrease at both walls. Dissipation adds heat internally, reducing normalized gradients at the hot wall but increasing temperature gradients toward the cold wall. The increased internal heating flattens velocity profiles, reducing both τ_1, and τ_2,. As porous resistance (σ) increases, we observe that τ_1, decreases at the left wall and τ_2, increases at the right wall, while Nu decreases at the left wall and increases at the right wall. Higher σ suppresses fluid motion within the porous medium, lowering shear and heat transfer on the hot wall.

7. Conclusion

The equations governing the fluid flow were nondimensionalized and later reduced to ordinary differential equations using similarity transformation. These equations (ordinary differential equations) with corresponding boundary conditions were solved using perturbation and BVP5C method. The effects of various controlling parameters on velocity, temperature, nanoparticles volume fraction, Nusselt number profile were discussed and presented graphically. The main findings of this research problem in this section are as follows:

Physical Insights:

1. An increase in the variable viscosity enhances the flow, while an increase in the variable thermal conductivity suppresses both the velocity and temperature. The ideal temperature and velocity are discovered for both water and copper based nano fluids. The flow is enhanced when the Brinkman number, the thermal Grashof number, and Casson parameter increases. When the Brinkman number increases, viscous dissipation becomes more significant. This generates additional heat within the fluid, which reduces resistance and allows the fluid layers to slip more easily, thereby enhancing the flow velocity. A higher thermal Grashof number indicates stronger buoyancy forces due to the temperature difference between the channel walls. These buoyancy forces act as a driving mechanism, pushing the fluid upward and thereby increasing the flow velocity. The Casson parameter is inversely related to plasticity, higher β reduces the yield stress, making the fluid behave more like a Newtonian fluid. As a result, the resistance to motion decreases, which enhances both velocity and temperature distribution.

2. Copper *cu* nanoparticles have very high thermal conductivity compared to the base fluid (water). When dispersed in water, they significantly increase the effective thermal conductivity, which enhances heat transfer between the channel walls and the fluid. This is why copper-water nanofluids generally exhibit the highest Nusselt number among common nanofluids.

3. This work considers Casson fluid behavior with variable viscosity and thermal conductivity in a vertical channel. The dual analytical–numerical approach provides reliable validation, while the comprehensive parametric analysis highlights the combined influence of buoyancy, dissipation, and nanoparticle loading. These insights are not only academically novel but also directly applicable to engineering systems such as cooling devices, biomedical flows and vertical heat exchangers.

Numerical observations

4. The combined use of perturbation methods and MATLAB's BVP5C solver offers high accuracy for steady-state analysis of Casson nanofluid flow, enabling detailed investigation of thermal and flow behavior under various physical effects.

5. The novelty of this study is in the combined effect of variable viscosity and thermal conductivity within a Casson nanofluid model and its demonstration of variable viscosity and thermal conductivity significantly enhances performance under buoyancy and dissipation effects. This dual-method approach ensures accuracy and strengthens the reliability of the findings which is less common in prior Casson nanofluid studies.

6. Our study systematically investigates the influence of Casson parameter, Brinkman number, Grashof number, nanoparticle fraction, and conductivity variation parameter on flow and thermal fields. Higher nanofluid volume fractions improve effective thermal conductivity, resulting in an enhanced Nusselt number. Simulations with –water nanofluid in a vertical channel indicate that increasing Grashof number and nanoparticle volume fraction not only improves heat transfer but also reduces entropy generation, meaning the process becomes more thermodynamically efficient.

7. This work contributes to the broader understanding of nanofluid behavior in vertical channel configurations offering a foundation for future studies incorporating complex boundary conditions and advanced materials.

8. Specifically, we now state that the present analysis is limited to steady state, 2D laminar Casson nanofluid flow with negligible magnetic induction effects and uniform nanoparticle dispersion, and does not include wall conduction, agglomeration or transient behavior. These clarifications are now included to clearly define the scope of the study and guide future research directions.

References

1. Mahanta, G., Shaw. S., *3D Casson fluid flow past a porous linearly stretching sheet with convective boundary condition*, Alex. Eng. J., 54, 653-659 (2015). https://doi.org/10.1016/j.aej

2. Kataria, H.R., Patel., *Radiation and chemical reaction effects on MHD Casson fluid flow past an oscillating vertical plate embedded in porous medium Radiation and chemical reaction effects on MHD Casson fluid flow past an oscillating vertical plate embedded in porous medium*, Alex. Eng. J., 55, 583–595 (2016). https://doi.org/10.1016/j.aej

3. Ramana Reddy, J., V., Anantha Kumar, K., Sugunamma, V., Sandeep, N., *Effect of cross diffusion on MHD non-Newtonian fluids flow past a stretching sheet with non-uniform heat A comparative study*, Alex. Eng. J., 57, 1829-1838 (2018). https://doi.org/10.1016/j.aej

4. Awais, M., Raja, M., A., Z., Awan, S., E., Shoaib, M., Ali, H., M., *Heat and mass transfer phenomenon for the dynamics of Casson fluid through porous medium over shrinking wall subject to Lorentz force and heat source/sink*, Alex., Eng., J., 60, 1355–1363 (2021). https://doi.org/10.1016/j.aej.10.056

5. Animasaun, Adebile, I., L., E., A., Fagbade A., I., *Casson fluid flow with variable thermo-physical property along exponentially stretching sheet with suction and exponentially decaying internal heat generation using the homotropy analysis method*, Journal of the Nigerian Mathematical Society,35, 1-17 (2016). https://doi.org/10.1016/j.jnnms

6. Pourmehran, O., Rahimi-Gorji, M., Ganji, D.,*Heat transfer and flow analysis of nanofluid flow induced by a stretching sheet in the presence of an external magnetic field,* J Taiwan Inst Chem Eng,16, 162–171 (2016). https://doi.org/10.1016/j.jtice

7. Mahanthesh, Shehzad, B., S., A., Gireesha, B., J., Shashikumar, N., S., Madhu, M., *Brinkman-Forchheimer slip flow subject to exponential space and thermal dependent heat source in a microchannel utilizing SWCNT and MWCNT Nano liquids*, Heat Transfer-Asian Research, 48(7), 1688–1708 (2019). https://doi.org/10.1002/htj.21452.

8. Abrar, A., Ali, Lara,J., Silvers., *The effect of temperature-dependent viscosity and thermal conductivity on the onset of compressible convection* , Geophysical and astrophysical fluid dynamics, vol. 115, no. 2, 207–220 (2021). https://doi.org/10.1080/03091929

9. Kuznetsov, A., V., Nield, D., A., *Natural convective boundary-layer flow of a nanofluid past a vertical plate*International Journal of Thermal Sciences, 49(2), 243–247 (2010). https://doi.org/10.1016/j.ijthermalsci.2009.07.015.

10. Hassan, A., Lawal, O., Amurawaye F.,*The Effect of Variable Viscosity on a Reactive Heat Generating Fluid Flow over a Convective Surface* , Journal of the Nigerian Mathematical Society 39 (1), 21-38 (2020). https://doi.org/10.15625/2525-2518/15296

11. Gbadeyan, J., A., Titiloye, E., O., Adeosun, A., T.,*Effect of variable thermal conductivity and viscosity on Casson nanofluid flow with convective heating and velocity slip* , open access article, 2405-8440 (2019). https://doi.org/10.1016/j.heliyon

12. Kalteh,M., *Investigating the effect of various nanoparticle and base liquid types on the nanofluids heat and fluid flow in a microchannel* , Appl. Math. Model 37, 8600–8609 (2013). https://doi.org/10.1016/j.apm

13. Haroon Ur Rasheed, Saeed Islam, Zeeshan, Waris Khan, Jahangir Khan, Tariq Abbas, *Numerical modeling of unsteady MHD flow of Casson fluid in a vertical surface with chemical reaction and Hall current*, Advances in Mechanical Engineering Vol. 14(3), 1–10 (2022). https://doi.org/10.1177/16878132221085429

14. Mabood, F., Khan, W., A., Ismail, A., I., M *MHD boundary layer flow and heat transfer of nanofluids over a nonlinear stretching sheet, a numerical study* , Journal of Magnetism and Magnetic Materials, 401, 159–168 (2016). https://doi.org/10.1016/j.jmmm

15. Shehzad, A., Hayat, T., Alsaedi, A., Obaidat, S *Effects of mass transfer and variable viscosity on MHD flow over a stretching sheet with chemical reaction* , Chemical Engineering Research and Design, 92(2), 302–310 (2015). https://doi.org/10.1016/j.cherd

16. Idowu, A., S., Falodun,B., O., *Variable thermal conductivity, and viscosity effects on non-Newtonian fluids flow through a vertical porous plate under Soret-Dufour influence*, Math. Comput. Simul, 177, 358–384 (2020). https://doi.org/10.1016/j.matcom

17. Kim, J., K., Jung,J., Y., Kang,Y., T., *The effect of nanoparticles on the bubble absorption performance in a binary nanofluid*, Int. J. Refrig, 29, 22–29 (2006). https://doi.org/10.1016/j.ijrefrig

18. Bahiraei, M., *Impact of thermophoresis on nanoparticle distribution in nanofluids*, Results in Physics, 7, 136–138 (2017). https://doi.org/10.1016/j.rinp

19. Samrat, S., P., Sulochana, C., Ashwinkumar G., P,*Impact of thermal radiation on an unsteady Casson nanofluid flow over a stretching surface*, Int J Appl Comput Math,5, 1–20 (2019). https://doi.org/10.1007/s42452-019-1656-0

20. Rawi, N.,A ., Ilias, M., R., Lim Y., J., *Unsteady mixed convection flow of Casson fluid past an inclined stretching sheet in the presence of nanoparticles*, J Phys Conf Ser, 890, 012-048 (2017). https://doi.org/10.1177/16878132221085429

21. Aziz,A., Alsaedi, A., Muhammad,T., Hayat, T.,*Numerical study for heat generation/absorption in flow of nanofluid by a rotating disk*, Results in Physics, 8, 785–792 (2018).

22. Umavathi, J., C., Syed Mohiuddin *Mixed convection flow of permeable fluid in a vertical channel in the presence of the first-order chemical reaction, variable properties* , variable properties. Special Topics, Reviews in Porous Media — An International Journal, 9(2), 155–176 (2018). https://doi.org/10.1615/SpecialTopicsRevPorousMedia.v9.i2.5

23. Buongiorno, J., *Convective transport in nanofluids*, Journal of Heat Transfer, 128(3), 240–250 (2006). https://doi.org/10.1115/1.2150834

24. Bhuvaneshwari R Havaleppanavar, Syed Mohiuddin, Anita Tuljappa, Karuna Prasad,M., Shaik Meera, D., *The Impact of Variable Viscosity and Variable Thermal Conductivity on the Mixed Convective Flow of Casson Nanofluid in a Channel with Chemical Reaction*, Journal of Advanced Research in Numerical Heat Transfer, 26(1), 44-66 (2024). https://doi.org/10.37934/arnht

25. Maziar Dehghan, Milad Tajik Jamal-Abad, Saman Rashidi,*Analytical interpretation of the local thermal non-equilibrium condition of porous media imbedded in tube heat exchangers*, Energy Conversion and Management 85, 264-271 (2014). https://doi.org/10.1016/j.enconman

6. Nomenclature

a	constant for viscosity (kg m^{-1} s^{-1})
b	characteristic length of the channel (m)
b_{v1}	viscosity variation parameter
b_{k1}	conductivity variation parameter
Br_1	Brinkman number
GR_{T1}	modified thermal Grashof number
Gr_{T1}	thermal Grashof number
g	acceleration due to gravity (m s^{-2})
k	thermal conductivity of the fluid (W m^{-1} K^{-1})
K_0	thermal conductivity at temperature T_0 (W m^{-1} K^{-1})
m	wall temperature ratio
Re	Reynolds number
T_0	reference temperature (K)
T	fluid temperature (K)
T_1, T_2	wall temperatures (K)
U_1	velocity (m s^{-1})
u	dimensionless velocity
$\bar{u}$	mean velocity (m s^{-1})
Y	coordinate axis (m)
y	dimensionless coordinate axis
Nu_x	Nusselt number (m^2 s^{-1})

Greek letters

β	Casson parameter
β_t	coefficient of thermal expansion (K^{-1})
θ	dimensionless temperature
μ	dynamic viscosity (kg m^{-1} s^{-1})
μ_0	dynamic viscosity at temperature T_0 (kg m^{-1} s^{-1})
ν	kinematic viscosity (m^2 s^{-1})
ρ	density of the fluid (kg m^{-3})
ρ_0	static density
ϕ	rescaled species concentration
τ_1, τ_2	skin friction
ΔT	difference in temperature
σ	porous parameter (m^{-2})
β_f	Thermal expansion coefficient of the base fluid (K^{-1})
β_s	Thermal expansion coefficient of solid nanoparticles (K^{-1})

Subscripts

f	quantities for base nanofluid
s	quantities for solid particles

Bhuvaneshwari R. Havaleppanavar,
Department of Mathematics,
K.L.E. Technological University,
Hubballi, Karnataka-580031, India.
E-mail address: bhuna27@yahoo.co.in

and

Syed Mohiuddin,*
Department of Mathematics,
Ballari Institute of Technology and Management,
Ballari, Karnataka-583104, India.
Affiliated to Visvesvaraya Technological University,
Belagavi–590018, India.
E-mail address: simoh14@gmail.com*

and

M. Karuna Prasad ,
Department of Mathematics,
Kishkinda University,
Ballari, Karnataka- 583120 India.
E-mail address: karunaprasad9@gmail.com

and

D. Shaik Meera,
Department of Mathematics
Ballari Institute of Technology and Management,
Ballari, Karnataka-583104, India.
E-mail address: skmeer7@gmail.com

and

Angadi Deepa N.,
Department of Mathematics
K.L.E. Technological University,
Hubballi, Karnataka-580031, India.
E-mail address: deepa.angadi@kletech.ac.in